Impact of Carbon Dust on Performance of Hall Heroult Cell: A Computational Analysis

Tushar Thorat[1], Amit Jha[2] and Amit Gupta[3]
1. Scientist
2. Senior Scientist
3. Lead Scientist
Aditya Birla Science & technology Company Pvt. Ltd. Taloja MIDC Panvel, Maharashtra, India.
Corresponding author: tushar.thorat@adityabirla.com

Abstract

Carbon dust in the cell adversely affects its current efficiency and specific energy consumption. Cells with higher level of carbon dusts may show symptoms like high bath temperature, red spots on steel shell, unusual variation in bath and metal height, anode spikes/mushrooms, etc. Unlike other impurities, carbon particles remain suspended in the bath which leads to an increase of electrical resistivity and emissivity. The rise in electrical resistivity leads to anode-cathode distance (ACD) squeeze, if the cell voltage is fixed. This scenario intensifies the heat generated per mm of ACD in the bath. Carbon dust floating on the surface of bath increases radiative heat loss. This may lead to localized cooling during cell operational activities causing reduced superheat which in turn leads to spike formation in newly set anodes. The mushrooms/spikes in the cell will cause localized heating due to uneven current distribution. To investigate the impact of squeezed ACD and mushroom/spike formation on the thermal balance of the cell, a computational study has been carried out. It was observed that, the bath temperature increases by 2 to 10 °C and shell temperatures increase by 30 to 40 °C. The ledge becomes thinner by around 3-5 cm due to localized heating. Effect of increased emissivity of bath on the radiative heat loss through exposed areas such as point feeder holes, open cavity during anode change, and tap hole was analyzed. This paper also describes the use of inferences drawn from these analyses to optimize the measures, like preheating of new anode or increase in anode set voltage, to compensate the increased heat loss.

Keywords: Carbon dust in aluminum reduction cells, Anode spikes, Heat balance, Radiative heat loss, Potshell temperature.

1. Introduction

Carbon dust in the cell adversely affects its current efficiency and specific energy consumption. Cells with higher level of carbon dusts may show symptoms like increased number of high bath temperature excursions (>970 ºC), red spots on steel shell, unusual variation in bath and metal height, anode spikes/mushrooms, etc. These abnormalities can further add to poor use of the manpower due to (1) increased frequency and duration of carbon dust skimming (2) increased time required to detect and remove the anode spikes [1] (3) maintaining bath height and (4) measurements, monitoring and other corrective actions.

Unlike other impurities in bath, the carbon dust particles either remain in suspended form or floats on bath top [2] [3]. Variation in concentration and particle size distribution of carbon in bath is given by Foosnaes et al [4]. The size of these carbon dust particles in bath can range from micrometers to centimeters with an average size of 10 micrometers. Coarser carbon dust particles float on the bath surface whereas finer dust particles remain suspended in bath [3]. Carbon dust in the bath can originate from (1) poor quality anode, (2) erosion of ramming paste seam, preformed carbon blocks at side lining and cathode blocks, (3) higher carbon percentage in

recycled anode cover material, (4) carbon fines captured by dry scrubbers returning to the cell through secondary alumina feeding, (5) stub protection material which is directly lost into bath [1], etc. One of the major issues associated with carbon dust is an increase of electrical resistivity of the bath. Based on the laboratory experiments, Bugnion et al. [3] reported that the electrical resistivity of bath can increase by 70 % if carbon concentration in bath increases from 0.06 % to 1.01 %. Foosnaes et al [4] presented computational study, complemented with plant scale experiment, reporting 6 % increase in bath resistance with 1 % carbon content. As bath resistivity increases, ACD gets squeezed to keep the voltage in set operating band. This effectively increases heat generated per unit depth of ACD. Such localized heating will impact bath temperature, side ledge thickness and the steel shell wall temperature.

The presence of carbon dust in the bath also increases the emissivity of bath by 23 % as reported by Bernd Rolofs [5]. Rise in bath emissivity will increase radiative heat loss from open cavity during anode change operation. Also, extra energy is supplied during anode change to compensate for heat loss and heat required by freshly installed 'cold' anodes to achieve the steady state temperature. Nevertheless, the increased radiative heat loss due to carbon dust will lead to localized drop in bath superheat. The decrease in superheat can lead to freezing of electrolyte on anode bottom surface causing uneven carbon consumption and eventually forming mushrooms or spikes [5], which are discussed in [6]. In older cells, lower superheat and lower ACD can cause more severe problems.

Poor control of cell thermal balance will intensify issues like mushroom formation, high bath temperature, low bath height, frequent jumps in excess AlF_3, etc. To investigate the thermal impact of increased bath resistivity, squeezed ACD, mushroom/spike formation and higher excess AlF_3, a computational study has been carried out and will be discussed in this paper. The effect of increased emissivity of bath on the radiative heat loss through exposed areas such as point feeder holes, tap holes and open cavity during anode change is analyzed through analytical calculations. This paper also describes the use of inferences drawn from these analyses to optimize the measures, like preheating of new anode or increase in anode set voltage, to compensate the increased heat loss.

2. Methodology

To illustrate the impact of increase in the bath resistivity and the anode spike on thermal balance and current distribution in a cell, thermoelectric simulations were carried out using a 3D finite element model in ANSYS APDL environment. This model was developed in the past for an 86-kA cell technology [8]. The same model was recalibrated for 235 kA cell technology. Model results were validated against thermal and electrical measurements, such as steel shell temperature, cathode voltage drop, electrolyte ledge profile, etc. To analyze impact of bath emissivity increase, an analytical equation is developed and used to quantify heat losses during anode change operation.

2.1 Increase of Bath Resistivity

Carbon dust content in bath considered for this study is in the range of 0.06 % to 1.01 %. The data of bath resistivities for different concentrations of the carbon dust in the bath are adopted from recent work by Louis Bugnion et al [3]. Based on the change in bath resistivity, ACD is being calculated for fixed bath voltage of 1.5 V and carbon content of 0.06 % (Case 1), 0.16 % (Case 2) and 1.01 % (Case 3). Case 1, case 2 and case 3 are analyzed for critical thermal parameters of the cell.

Thermo-electric simulations were carried out to analyze cumulative impact of presence of carbon dust and high excess AlF_3 content in bath. Liquidus of the bath at AlF_3 content of 15 % is

calculated using equation given by Solheim et al. [14]. Bath resistivity and ACD were considered for carbon concentration of 1.01 %.

2.2 Bath Resistivity Increase

Total heat demand during anode change operation is calculated by using Equation 1. Heat demand for clean bath and dirty bath is compared to analyze impact of carbon dust on bath temperature decrease during anode change operation. Heat loss from the alumina feeding holes and the tap hole can increase heat demand of a cell. Analytical calculations are performed to study these factors.

Over all heat demand during any anode change operation can be written as:

Heat demand due to anode change operation = Heat demand of 'cold anode' + Overall (Convective + Radiative) heat loss from open cavity

Mathematically:

$$Q_{loss} = \int_{T_{ai}}^{T_{af}} M_a C_a dT + \int_{T_{pi}}^{T_{pf}} M_p C_p dT + \left[A \times \varepsilon \times \sigma \times \left({T_s}^4 - {T_o}^4\right) \times (t \times 60)\right] + [h \times A \times (T_s - T_o) \times (t \times 60)] \quad (1)$$

where:

M_a	Mass of anodes in kg
C_a	Specific heat of anode material in J/kg°C
T_{af}	Final (Steady state) Temperature of anode in °C
T_{ai}	Initial temperature of anode in °C
A	Area of open cavity (during anode change) in m^2
ε	Emissivity of bath (0.65 for clean bath, 0.8 for dirty bath)
σ	Stephen Boltzmann constant in W/m^{2}K^4
T_s	Temperature of surface of bath in K
T_o	Ambient temperature above bath surface in K
h	Convective heat transfer coefficient in W/m^{2}K
M_p	Mass of anode stub in kg
C_p	Specific heat of steel J/kg°C
T_{pf}	Final (Steady state) temperature of stub in °C
T_{pi}	Initial temperature of stub in °C
t	Time between removal of used anode and placing new anode in min (30)

Heat capacity of anode material is calculated using equation 2 obtained from JANAF data.

$$C_a = (9.06 \times 10^{-7} \times T^3) - (2.77 \times 10^{-3} \times T^2) + (3.15 \times T) + 631 \quad (2)$$

Heat capacity of stub material is calculated using equation 3 obtained from data given by Andrea Lucherini [16].

$$C_p = (2.22 \times 10^{-6} \times T^3) - (1.69 \times 10^{-3} \times T^2) + (0.773 \times T) + 425 \quad (3)$$

2.3 Anode Spikes

As describe earlier, increased heat loss due to presence of carbon dust favors the formation of anode spikes in the cell. Impact of the anode spikes, on thermal balance and current distribution in the cell, is studied by a steady state thermo-electric analysis.

2.4 Impact of Carbon Dust in a Cell Operating at Higher Excess AlF_3

In a normal scenario, most of the smelter potlines operate at bath ratio of 1.1 to 1.15 or excess AlF_3 of 10-12 %. However, it is observed that, in certain conditions excess AlF_3 concentration in some cells can increase up to 14-15 % or go down to 7-8 %. To understand impact of such extreme variations, 15 % excess AlF_3 is considered.

Liquidus temperature of the bath with 15 % excess AlF_3 is calculated using the equation developed by Solheim et al. [14]. The impact of lower liquidus temperature along with increase in bath resistivity is analyzed by steady state thermo-electric model.

3. Results and Discussion

Findings from computational analysis of the 4 scenarios described in previous section are described and discussed in this section.

3.1 Impact of Bath Resistivity Increase

Based on bath resistivity change, ACD is calculated for fixed bath voltage drop of 1.5 V. These calculated values of ACD are given in Table 1.

Table 1. Variation in electrical resistivity and ACD with carbon dust mass % in bath.

Case No.	Mass % C in the bath	% resistivity increase	Electrical resistivity	ACD (mm)
1	0.06	0	0.0046	43.8
2	0.16	13	0.0052	37.8
3	1.01	68	0.0077	25.6

Ledge profiles obtained from thermo-electric analysis are plotted in Figure 1. Due to increased heat generation per unit depth of bath in the region between the anode and the cathode, the ledge near the metal-bath interface reduces. As a result, the ledge ~5 cm thinner than in case 1 is obtained for case 3. The ledge toe profiles obtained for case 2 and 3 are moved to near the corner of the ramming paste seam. Any further melting of the ledge can pose the threat of lining erosion due to direct contact between liquid aluminium and the ramming paste seam. Maximum sidewall steel shell temperatures increased from 320 ºC (Case 1) to 325 ºC (Case 3).

It is also noteworthy that, ACD in case 3 drops to 27 mm. Such a low ACD leads to noise and shakiness of the cell. In a recent study it was reported that, for cells operating at 0.07 % carbon in the bath, noise level of 20 mV was reached at 14 mm ACD squeeze. However, for cells operating at 0.11 % the same noise level was reached at 6 mm ACD squeeze [2]. Such scenario results in low current efficiency (CE) and hence, forces the operator to raise the set voltage of the cell. Higher set voltage increases heat generation in the cell and increases bath temperature. High bath temperature favors the CO_2 reactivity of carbon anode and hence leads to higher net carbon consumption and dust generation in the cell. This vicious cycle of the carbon dust forces the operator to skim the dust at frequent intervals to avoid CE loss.

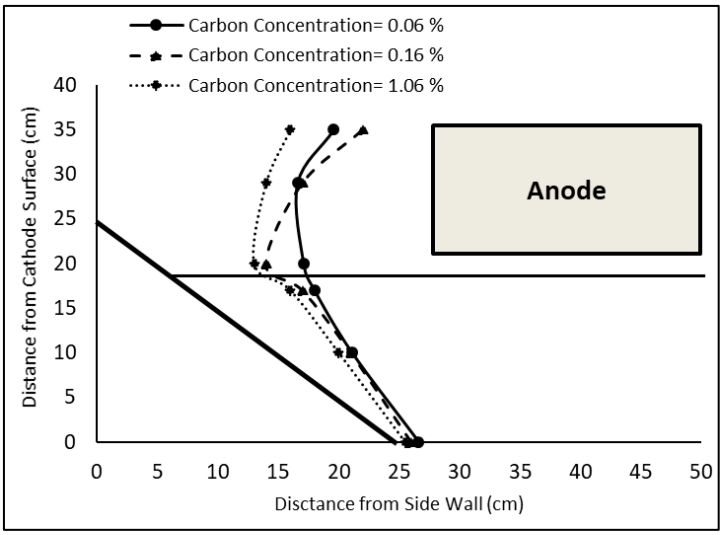

Figure 1. Ledge profiles obtained for CASE 1, CASE 2 and CASE 3.

3.2 Impact Bath Emissivity Increase

Summary of analytical calculations with Equation (1) for the cell under study is given in Table.2.

Table 2. Heat demand in one anode change operation.

Heat losses from Open Cavity			
	Unit	**Clean bath**	**Dusty bath**
Area of open cavity	m^2	1.81	1.81
Heat transfer coefficient	W/m^2K	6.2	6.2
Duct gas temp	°C	200	200
Bath temperature	°C	965	965
Heat loss by convection	W	8612.99	8669.28
	MJ	15.50	15.60
Heat loss by radiation			
Area open cavity	m^2	1.81	1.81
Emissivity		0.65	0.8
Stephen Boltzmann Constant	W/m^2K^4	5.67E-08	5.67E-08
Heat loss by radiation	kW	153.86	192.51
	MJ	276.95	346.52
Total Heat Loss from open cavity	MJ	292.45	362.12
Enthalpy for heating new anode			
New anode temperature	°C	50	50
Weight of new anode	kg	1617	1617
Average temperature anode at steady state	°C	800	800
Weight of stub	kg	165	165
Heat required for heating new anode	MJ	1775.613	1775.613
Heat required for heating new stub	MJ	30.984	30.984
Total Heat requirement during one anode change operation	**MJ**	**2099.049**	**2168.722**

Total heat demand in case of dirty bath, during anode change operation, increases from 2099 MJ to 2169 MJ. This rise in heat demand can be attributed to increase in radiative heat loss and convective heat loss from open cavity. This can lead to 11 °C temperature drop or increase in under-freeze in bath. In cells operating at lower superheat and lower anode to cathode distance, this scenario can lead to issues like anode spikes. One should consider this while deciding set voltage during anode change operation. In present case study, it is required to modify the anode change set voltage program to enable it to provide additional 20 kWh of energy.

Analytical calculations were performed to find out impact of carbon dust on radiative heat loss from tap hole and feeder holes. It was found that for a cell with dirty bath, the heat loss increases by 1030 W. This demands increasing set voltage by 5 mV to maintain the same superheat and stability of the cell.

3.3 Impact of an Anode Spike

A significant number of anode spikes (1200) were reported in Vorde smelter during low superheat (due to presence of the carbon dust) operation. 78 % of all anode spikes were found in the region closer to side wall, due to relatively lower superheat in the region. Based on these findings and anode spike dimensions reported by authors [5], anode spike geometry illustrated in Figure 3 is considered for thermoelectric simulation.

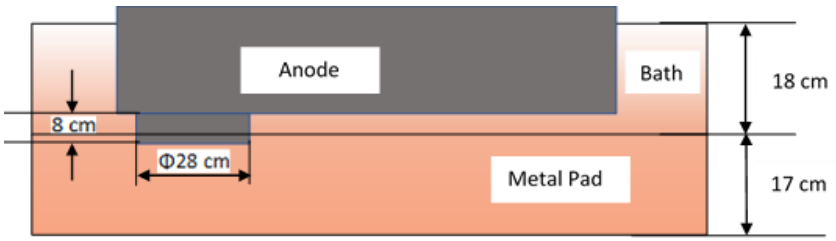

Figure 3. Schematic showing position and geometry of anode spike.

Due to the immersion of anode spike in the metal pad, short-circuit happens. As a result, almost all the current starts flowing through the anode spike. The change in current distribution in presence of anode spike can be seen in Figure 4.

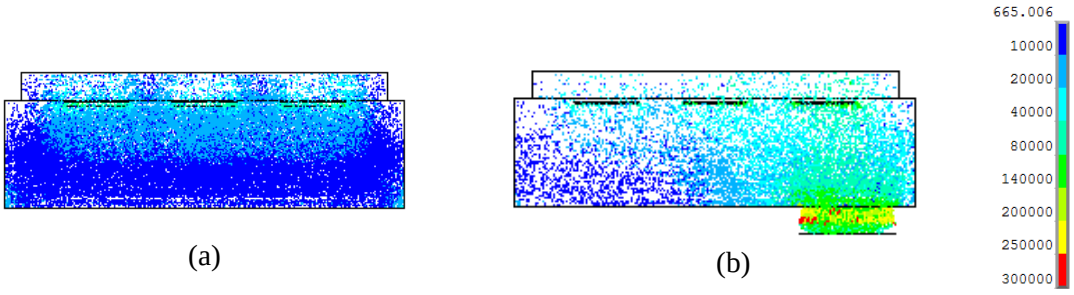

Figure 4. Current distribution in the cell. Left: Anode without spike, Right: Anode with spike.

In normal cell operation all anodes have a uniform current density of ~8500 A/m^2. Spike immersed in the metal pad creates a secondary path for the current flow. Hence, current density in the anode with a spike increased to a value of ~280 000 A/m^2. This current flow pattern results in localized heating and can lead to bath temperature rise to ~1000 ºC and melting of ledge in the nearby region of the spiked anode. The same can be observed in Figure 5. Such abrupt thermal excursions may cause cracking inside anodes. Increase in time of contact of anodes with the metal,

and of the anode temperature accelerates anode reactivity [15] and, hence, increases the net carbon consumption.

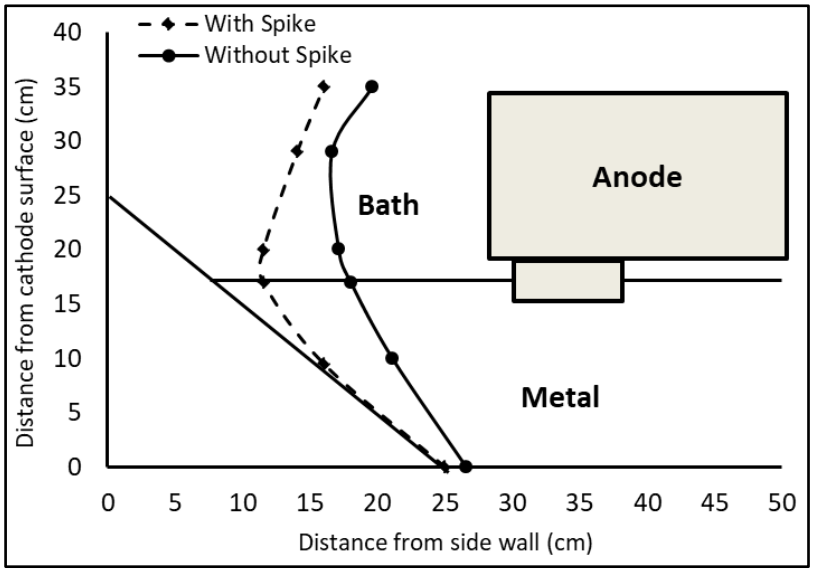

Figure 5. Ledge profile in the presence of an anode spike.

Such occurrence of anode temperature rise is reported in the past by Frank Aune et al [9]. No ledge was observed near the toe of ramming paste seam and molten aluminium was in direct contact with the lining. At the same time, due to current density decrease in other anodes, bath temperature in the areas away from the spiked anode started decreasing and hence reduced the bath superheat. Steel shell temperature in the region around the anode spike also increased from 325 ºC to 381 ºC. A comparison of the shell temperature in normal cell operation and anode spike scenario is given in Figure 6.

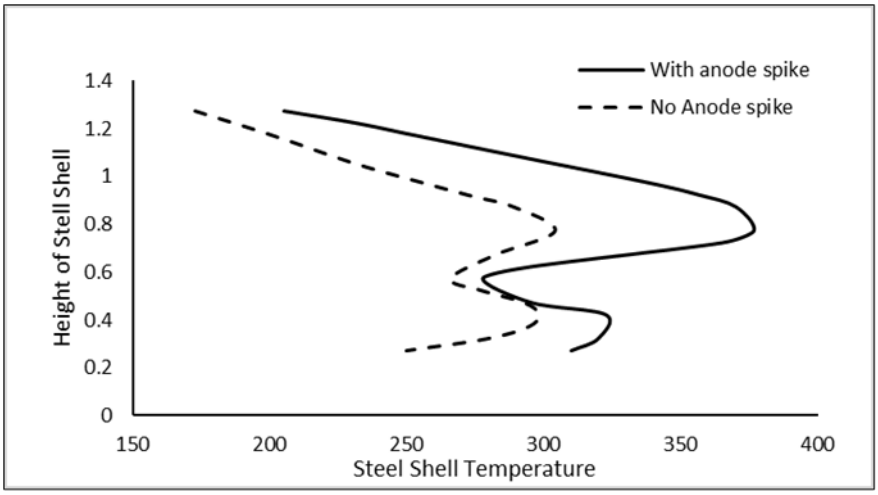

Figure 6. Impact of anode spike on steel shell temperature.

Such situations can cause heavy CE loss in and threatens lining erosion. Hence, this situation demands immediate replacement of the spiked anode.

3.4 Impact of Carbon Dust in Cell Operating at Higher Excess AlF_3

Ledge profiles obtained as a result of computational analysis of a cell running at high excess AlF_3 with carbon concentration of 1.06 % is given in Figure 7. Lquidus temperature of bath at higher excess AlF_3 (15 %) content drops to ~928 ºC. This change in liquidus temperature resulted in thinning of electrolyte ledge by 3-4 cm. Increase bath resistivity due to presence of carbon dust adds more trouble to this problem. As a cumulative impact no ledge is observed in the metal pad region near the sidewall. As discussed earlier, to operate a cell without noise, the operator must raise the set cell voltage. The rise in set voltage can further increase heat generation in the cell and, thus, increase the severity of lining erosion. In worst case scenario, this can cause cell tap-out from side walls.

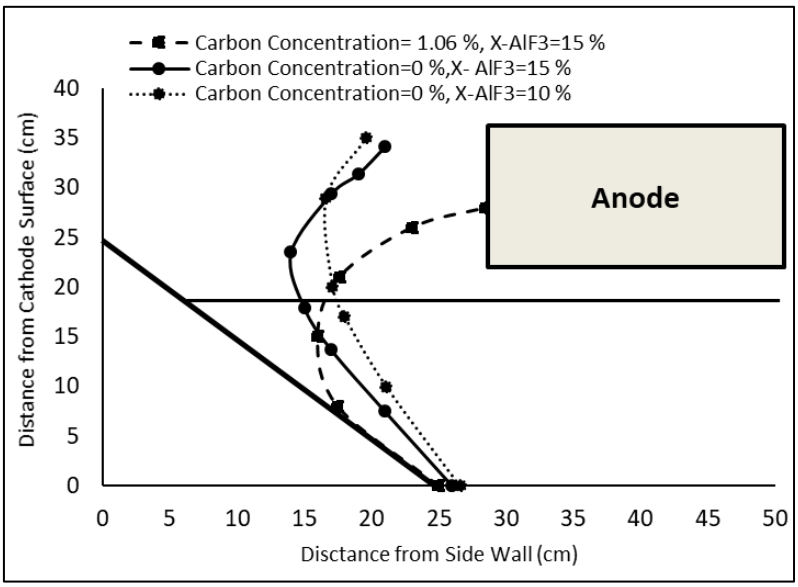

Figure 7. Ledge profile for cell operating at 1.06 % C and 15 % excess AlF_3.

4. Conclusions

Based on the computational analysis and analytical calculations performed to study the impact of carbon dust on thermal performance of cell, the following observations were made:

1. Impact of increased bath electrical resistivity in the Hall Héroult cell is analyzed with thermo-electric simulations. It was observed that at carbon content of 1 % the ledge thickness reduces by 5 cm. At the same time, the temperature of the side wall steel shell increases by 5-7 ºC. In the presence of excess AlF_3 of 15 %, this issue becomes more severe and significant reduction in ledge thickness was observed in the metal pad region. This may increase the chances of sidewall failure.
2. Heat loss in anode change operation was calculated and compared for 'clean bath' and 'dirty bath' situations in the cell. Because of higher emissivity of bath, heat losses in 'dirty bath' scenario increased by 3-4 % in comparison with the 'clean bath'. This would lead to 10-11 ºC bath temperature drop, which may result in negative superheat and increased under-freeze after anode change, which can ultimately lead to anode spike formation.
3. Impact of an anode spike on thermal balance and current distribution in the cell was analyzed. Anode current density in the spike region may increase drastically up to ~25 times. This causes localized heating; thus, no ledge was observed in the area adjacent to ramming seam. Steel shell temperature in this region increases by 55 ºC. This kind of scenario demands immediate replacement of the spiked anode and frequent carbon dust skimming to avoid major loss in performance.

5. References

1. Neal Wai-Poi and Bernd Rolofs, Impact of energy management and superheat on anode spike formation, *Light Metals* 2002, 535-539.
2. Louis Bugnion and Jean-Claude Fischer, Effect of carbon dust on the electrical resistivity of cryolite bath, *Light Metals* 2016, 587-591.
3. Kai Grjotheim, Berry Welch and Mark Taylor, Relating operating strategy and performance in Aluminium Smelting cells-an overview, *Light Metals* 1989, 255-260
4. T. Foosnaes T et al., Anode dusting in Hall Heroult Cell, *Light Metals* 1986, 633-642.
5. Bernd Rolofs and Neal Wai-Poi, The effect of anode spike formation on operational performance, *Light Metals* 2000, 189-193.
6. Mohamed Ali and Abdel-Masser Omran, Anode spike formation in prebaked aluminium reduction cells, *Al-Azhar Engineering 12th international conference* 2012, 30-36.
7. Ali Jassim et al., Studies on preheating using individual anode signals in Hall-Heroult reduction cells, *Light Metals* 2016, 623-628.
8. Amit Gupta and Sankar Nambuthiri, Impact of carbon seam on freeze profile in aluminium reduction cells, *Transactions of Indian Institute of Metals* , Vol 6, 2017, 1-12.
9. Frank Aune et al., Thermal effects by anode changing in prebake reduction cells, *Light Metals 1996, Essential Readings in Light Metals* Vol 2 2016, 562-568.
10. Matthias Dechent et al., Carbon dust-Its short term influence on potroom operations during anode change, *Light Metals* 2021, 384-391.
11. Warren Haupins, Principles of aluminium electrolysis cell, *Light Metals* 1995, 195-203.
12. Khalil Khaji and Mohammed Qasseni, Role of anode manufaturing process in net carbon consumption, *Metals* 2016 Vol 128, 127-138.
13. R Ødegård, A Solheim and K Thovsen, Current pickup and temperature distribution in newly set prebaked Hall Heroult anodes, *Light Metals* 1992, 555-560.
14. A Solheim et al., Liquidus temperature and alumina solubility in the system Na_3AlF_6-AlF_3-LiF-CaF_2-MgF_2, *Light Metals* 1995, 451-460.
15. S.G. Shahrai et al., Quality of anode, Overview of problems and some methods of their solution, Part 1, Coal foam in aluminium electrolyzer, *International journal of applied engineering research*, Vol 12, Nov 2017, 8976-8985.
16. Andrea Lucherini, Experimental study of the behavior of steel structures protected by different intumescent coatings and exposed to various fire scenarios, *PhD Thesis, Department of Civil Engineering, Technical University of Denmark*, 2015-2016.